Geophysical Research Letters

Supporting Information for

Northern Galápagos corals reveal twentieth century warming in the eastern tropical Pacific

Gloria Jimenez[1], Julia E. Cole[2], Diane M. Thompson[3], Alexander W. Tudhope[4]

[1]Department of Geosciences, University of Arizona, Tucson, Arizona, USA.

[2]Department of Earth and Environmental Sciences, University of Michigan, Ann Arbor, USA

[2]Department of Earth and Environment, Boston University, Boston, Massachusetts, USA.

[3]School of Geosciences, University of Edinburgh, Edinburgh, Scotland, UK.

Contents of this file

Additional Supporting Information (files uploaded separately)

Introduction

The following Supporting Information includes additional information on the climate and oceanographic setting of the eastern tropical Pacific, coral collection and processing, geochemical analyses, Sr/Ca-SST calibration, and a comparison of trends in the individual coral cores used to create the Wolf composite reconstruction. Data for the Wolf composite reconstruction (including the individual coral cores used in the composite) are presented in Table S2.

Text S1.

Climate and oceanographic setting of the Galápagos Islands and eastern tropical Pacific

Wolf Island is located at 1.4°N, 91.8°W. Based on high-resolution Optimum Interpolation Sea Surface Temperature (OISST) (Reynolds et al., 2007) data from 1982-2014 for the 0.25x0.25-degree grid box centered on 91.875°W, 1.375°N, Wolf Island has a seasonal SST range of approximately 2.5°C and an annual mean SST of 25.5°C (Fig. 1a). The warmest month of the year is March, with an average SST of 27.2°C, and the coolest month is August, with an average SST of 24.3°C.

Ocean climatology near the Galápagos and throughout the eastern tropical Pacific (ETP) is influenced by several prominent features. The equatorial front demarcates the northern boundary of the cold tongue and divides warm, low-salinity Tropical Surface Water to the north from cooler, higher salinity Equatorial Surface Water to the south. Surface currents in the area include the westward-flowing North Equatorial Current (NEC), which is fed by the eastward-flowing North Equatorial Countercurrent to the south (NECC; eastward surface flow from 2-10°N) and the California Current to the north (Fig. S1; Toggweiler and Dixon, 1991; Fiedler and Talley, 2006). Closer to the equator is the westward-flowing South Equatorial Current (SEC), which receives water from the Peru Current (PC) and recirculation from the NECC (Lukas, 1986; Kessler, 2006). The northern SEC(N) branch includes flow between the equator and the NECC; the southern SEC(S) includes flow between the equator and 8°S. Although the Galapagos lie primarily in the SEC region, the complex topography and strong seasonal to interannual variations in ocean climate near the Galápagos create highly variable flow within the archipelago.

Below these surface currents, dashed lines show the subsurface Equatorial Undercurrent (EUC; eastward flow between 2°S and 2°N), which slows and shoals in the ETP, causing a downstream decrease in the temperature of the cold tongue (Fiedler and Talley, 2006; Kessler, 2006). At approximately 92°W, the EUC diverts around the Galápagos platform; there is general agreement that significant flow moves south of the islands, but it is less clear whether any flow proceeds north of the islands or is reflected (Strub et al., 1998; Kessler, 2006). South of the islands, upwelling drains the upper layers of the EUC; the lower layers continue east to contribute to the southward Peru Undercurrent (PUC) near the South American coast. Additionally, some portion of the EUC recirculates to supply the South Equatorial Current (SEC; Lukas, 1986; Kessler, 2006). From April to May, the EUC reaches the surface at 110°W, reversing the usually westward surface flow (Johnson et al., 2002; Kessler, 2006).

The dominant surface winds in the ETP are the easterly trades associated with the Walker circulation (Fig. 1a; Julian and Chervin, 1978; Wallace et al., 1989). In the cold tongue area, these originate in the Southern Hemisphere and join the Intertropical Convergence Zone (ITCZ) north of the equator (Wallace et al., 1989). Winds are closely coupled with SSTs, driving

upwelling in the cold tongue region (Zhang and McPhaden, 1995) but also responding to changes in underlying SSTs (Wallace et al., 1989).

Sample processing

Wolf Island cores GW10-3 and GW10-10 were halved, slabbed, and cleaned by sonication in deionized water. The slabs were X-rayed, and the resulting images were used to establish sampling transects along the coral's primary growth axis (Fig. S2). The transects were then milled continuously in 1 mm increments using a Sherline Computer Numerical Control (CNC) automated benchtop mill. The sample tracks were 4 mm wide and 2.5 mm deep.

Several sections of the cores were examined with a scanning electron microscope (SEM) at the University of Arizona to determine whether the skeleton had experienced alteration or diagenesis (Sayani et al., 2011). For comparison, we selected areas that appeared unaltered, areas with visible discoloration or disturbances such as death horizons or nearby gastropod borings, and areas with anomalously low Sr/Ca values. We assessed the images for the presence of secondary aragonite, dissolution, and infilling.

SEM images of both coral skeletons display pristine, primary material that has not been affected by diagenesis or alteration (Fig. S2). An exception is the death horizon area of GW10-3, which is visibly altered and remineralized; the SEM image of this area shows acicular aragonite crystals indicative of secondary cement infilling (Sayani et al., 2011). We did not sample this area for Sr/Ca-SST reconstruction.

The interval from 1968-1974 in core GW10-3 displays a stunted seasonal cycle with a limited temperature range compared to the rest of the record. X-rays show disorganized skeletal architecture in this section of the coral, with corallites converging or growing in a direction that is not parallel to the slab. This subparallel growth can bias coral Sr/Ca measurements in both a positive and negative direction (DeLong et al., 2012). Therefore, caution should be used when interpreting results on subannual to shorter timescales over this interval.

Geochemical analysis and chronology construction

Sr/Ca elemental analyses followed the methodology of Schrag (1999). For each sample of coral powder, 0.35-0.45 mg was acidified in 2 mL of 5% trace metal grade HNO_3 to achieve a dilution of approximately 80 ppm Ca. The ratio of Sr (at 407.77 nm) to Ca (at 393.37 nm) was measured on a Jobin-Yvon Optima 2C inductively coupled plasma atomic emission spectrometer (ICP-AES) at the University of Arizona. A reference solution was measured between samples to monitor analytical drift. Five high purity standards and an in-house coral reference standard were measured every 60 samples; the standard deviation of the in-house standard was 0.022 mmol/mol over all the sample runs. The average method detection limit of the ICP-AES was 0.033 mmol/mol.

Age models for the cores were determined based on seasonal cycles in the Sr/Ca time series, as well as density banding. Seasonal Sr/Ca minima were identified throughout the record and used as age model tie points; these correspond to temperature maxima, which we tuned to

March of each year (the month with the warmest average SST). The series were converted to the time domain by linear interpolation between tie points using the Ager and Timer programs in the Arand software package (Howell et al., 2006). Age models were checked and refined using density banding and major historical El Niño events.

We created a monthly composite record that combined data from the two cores. For each core, we standardized the data by subtracting the mean and dividing by the standard deviation. We then averaged these standardized values over the periods of overlap between the cores (Oct. 1982-Dec. 1975 and May 1987-Mar. 2010). Finally, we converted the composite record back to Sr/Ca values using the average and standard deviation over both cores (cf. Mann and Jones, 2003).

Sr/Ca-SST calibration and uncertainty calculation

We used weighted least squares (WLS) regression to calibrate the Sr/Ca concentration of the Wolf Island coral composite to SST (Thirumalai et al., 2011). We regressed the Sr/Ca composite against the OISST grid box centered over Wolf Island (91.875°W, 1.375°N) across the most recent time period of continuous overlap between the cores (May 1987-March 2010).

WLS regression yielded the equation Sr/Ca = 10.66-0.057*SST, which is consistent with the general equations suggested by Gagan et al. (2012) and Corrège (2006) (Supp. Table 1). Reduced major axis (RMA) regression gave similar results (not shown).

The two cores overlap well over their calibration interval from 1987-2010 (with a Pearson product moment correlation of $r=0.71$ and $p<0.001$), and the difference in their means over this interval amounts to 1.1 °C. This difference is small compared to the SST variability reflected by both cores (2-6°C; Table S1 and Fig. 2) and is well within the range reported by previous studies (e.g., DeLong et al., 2007; Linsley et al., 2008; Wu et al., 2014). Differences in Sr/Ca between the two colonies could be caused by microenvironmental variations between their sites or vital effects due to the difference in core extension rates (Table S1; Wu et al., 2014).

We propagated error in our Sr/Ca-SST estimates following Nurhati et al. (2011). These calculations consider the uncertainty associated with analytical precision and Sr/Ca-SST calibration. The error associated with the trend is smaller than absolute error estimates because uncertainty associated with the intercept of the Sr/Ca-SST equation does not affect relative changes in Sr/Ca-SST (Nurhati et al., 2011).

Comparison of trends in individual Wolf coral cores

We present the trend in the Wolf composite reconstruction in the main text (Fig. 4). Below, we evaluate trends in the two cores that contributed to the composite (GW10-3 and GW10-10) separately.

Analyzing the cores individually shows that the significant warming trend in the Wolf composite (Figs. 4 and S5) is driven by the trend in the longer of the two cores, GW10-3 (with a

length of 71 years; Fig. S6). SiZer indicates significant warming trends in GW10-3 on both a 10-year timescale (beginning in 1976) and a 50-year timescale (beginning in 1940). For core GW10-10 (with a length of 35 years), while SiZer detects a warming trend throughout the series, it does not pass significance testing (Fig. S6).

The lack of a significant trend in core GW10-10 is related to its higher variability and shorter length. The core grew faster than GW10-3 and suggests higher-amplitude SST variability (compare family plots with blue lines in Fig. S6). The high variability in GW10-10 mitigates the significance of shorter term trends.

However, the family plot for GW10-10 (Fig. S6) clearly suggests the presence of an increasing trend on longer timescales. If GW10-10 had included more data prior to 1976 (when it began growing), this trend would probably have passed SiZer's significance criteria despite the higher variability in the coral record.

We chose to present and analyze the composite of cores GW10-3 and GW10-10 because this likely constitutes a better reflection of the true SST variability and trends in the area. After analyzing both the composite and the separate cores, we suggest that the significant warming trend apparent in the Wolf composite reconstruction is reliable despite the fact that the shorter of the coral records it includes (GW10-10) does not show significant trends on its own.

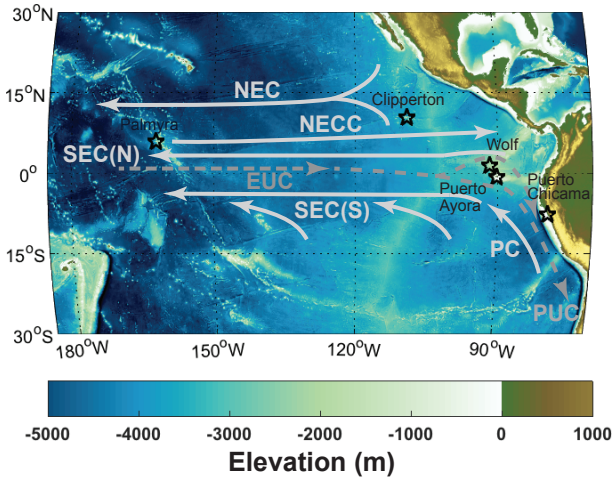

Figure S1. Oceanographic setting of the ETP, with bathymetry from the National Geophysical Data Center 2-minute Gridded Global Relief Data (ETOPO2) v2 (2006). Arrows schematically show major currents: the surface North Equatorial Current (NEC), North Equatorial Countercurrent (NECC), northern and southern branches of the South Equatorial Current (SEC(N) and SEC(S)), and the Peru Current (PC); and the subsurface Equatorial Undercurrent (EUC) and Peru Undercurrent (PUC). Stars indicate coral and instrumental sites.

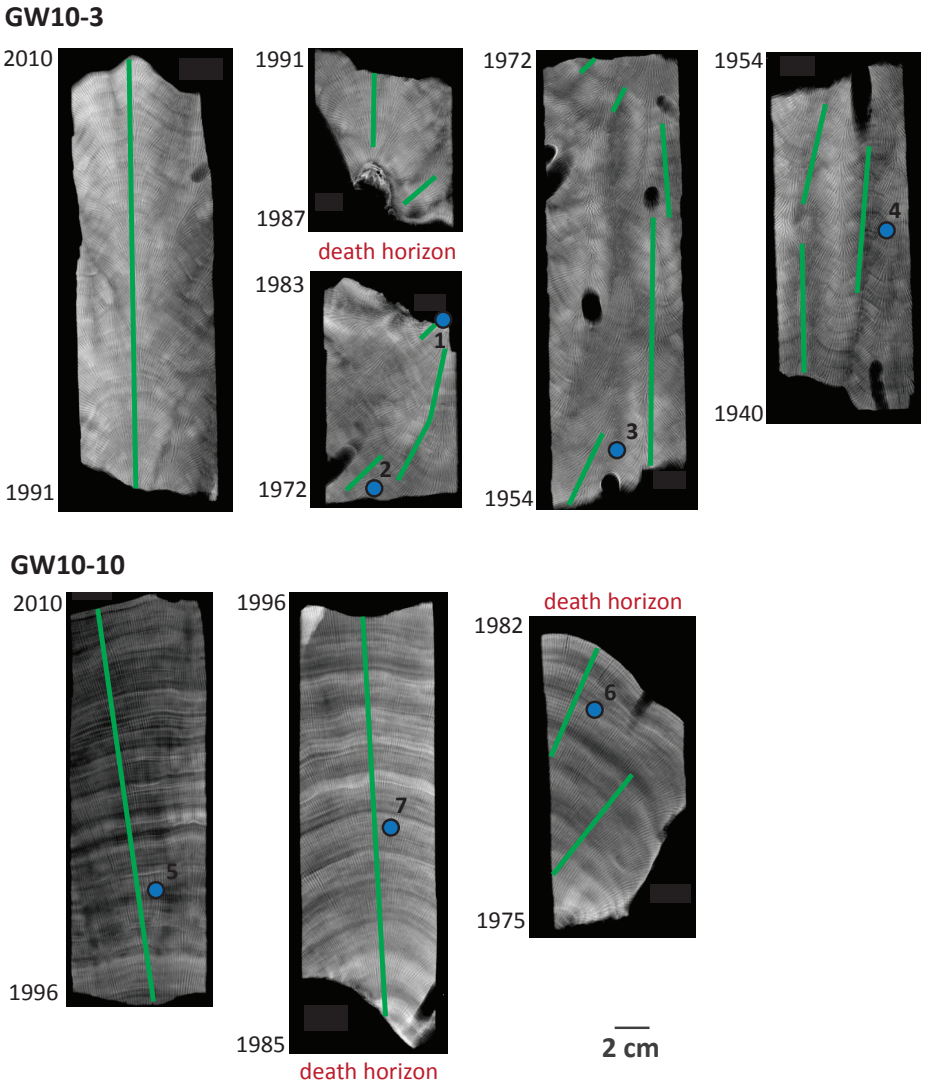

Figure S2. X-ray images of Porites spp. slabs live-cored from Wolf Island; GW10-3 spans 1940-2010 (upper panel) and GW10-10 spans 1975-2010 (lower panel). Green lines indicate sampling paths, which were taken parallel to the coral's primary vertical growth axis when possible. Red text marks the 1982-83 death horizon in both cores; numbered blue dots are SEM sample locations.

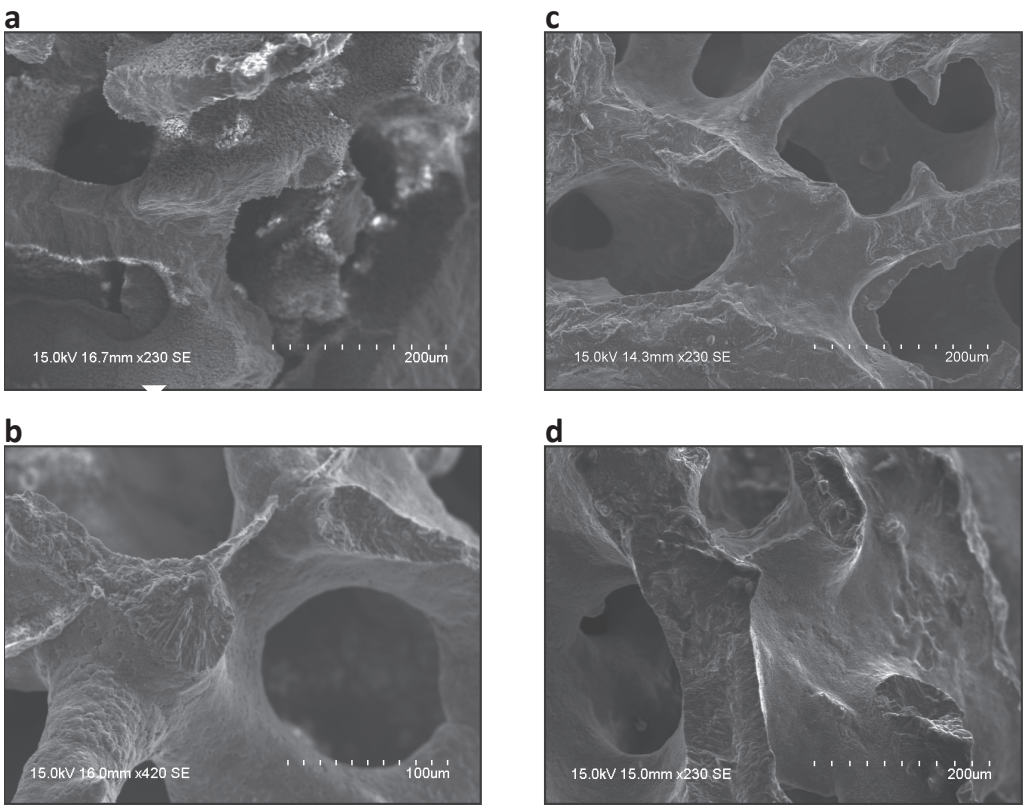

Figure S3. Scanning Electron Microscopy (SEM) images of Wolf coral cores; scale indicated on images. See Fig. S1 for sample locations on cores. (a) Sample 1, from the 1982-83 death horizon in GW10-10 (not sampled for Sr/Ca), shows acicular aragonite crystals indicative of secondary alteration (white arrow points to one surface with secondary aragonite growth); (b) Sample 2, from a sequence in GW10-3 with a stunted seasonal cycle; shows primary aragonite; (c) Sample 3, from a cold anomaly in GW10-3 corresponding to the 1955-56 La Niña; shows primary aragonite; (d) Sample 7, from a sequence in GW10-10 with a strong seasonal cycle, shows primary aragonite.

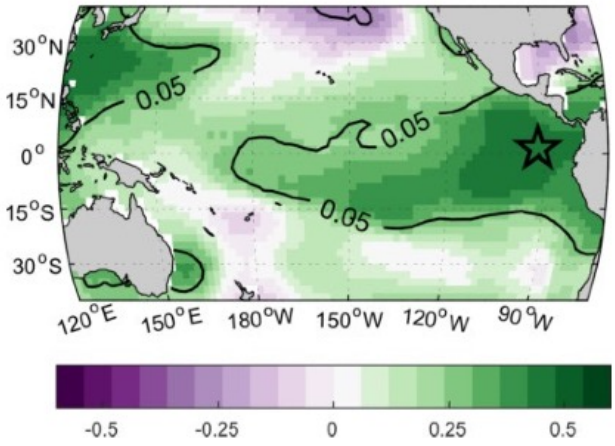

Figure S4. Correlation map showing the Pearson correlation coefficient between the Wolf composite time series (location marked with a star) and the ERSST4 field. Both datasets were averaged over April-March tropical years from 1940-2010. Colors indicate the strength of correlation and contours indicate significance at $p<0.05$, adjusted for autocorrelation between points in the field.

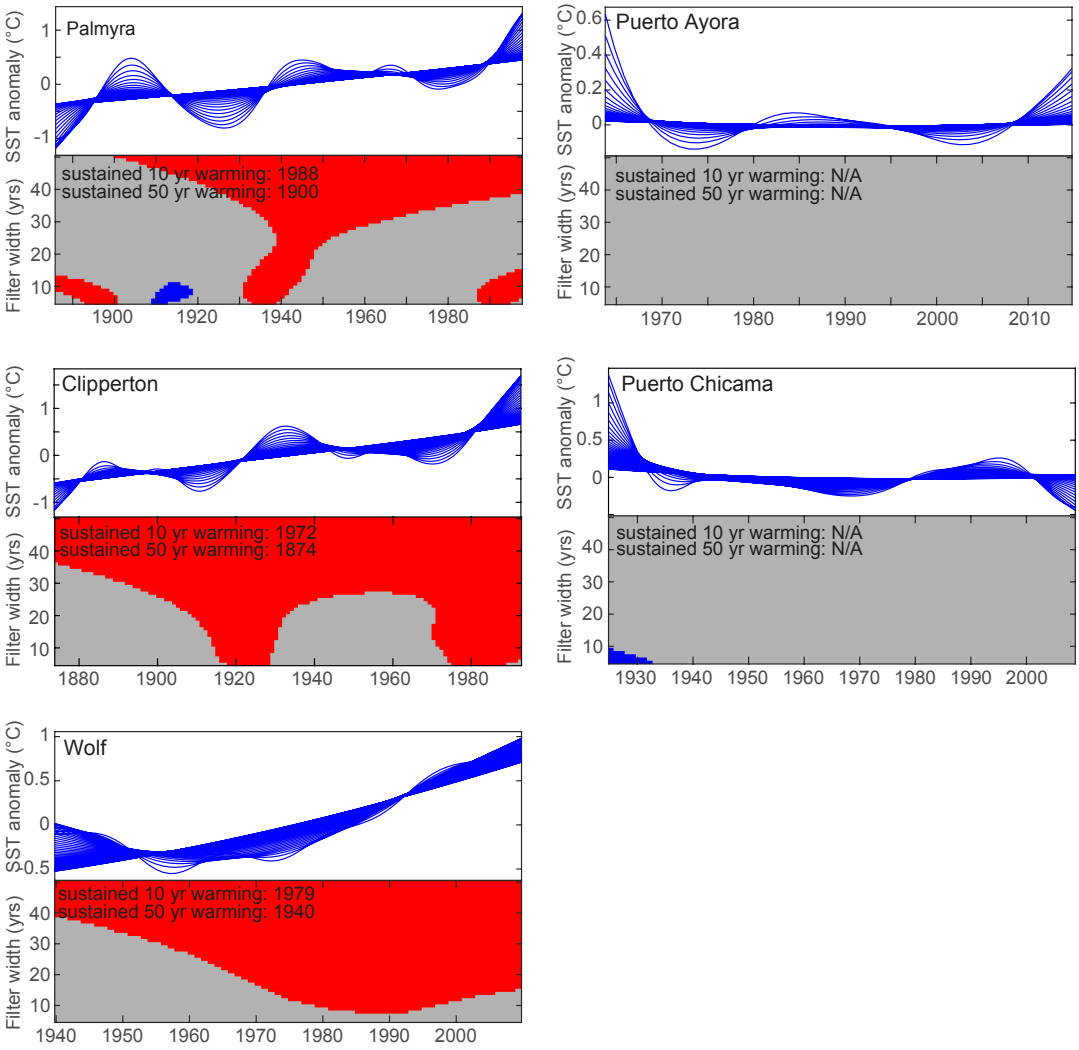

Figure S5. SiZer plots for ETP coral and instrumental data series (averaged over tropical years, from April-March). For each site, the upper panel (white background with blue lines) shows the family of Gaussian kernel smooths that constitute the target of SiZer analysis (including filter widths from 5-50 years). The lower panel (red, blue, and grey shapes) shows "SiZer maps" that visually represent SiZer's results. The color of each pixel at a given year and filter width reflects SiZer's hypothesis testing for that location and resolution; significant warming is shown in red and significant cooling in blue (evaluated at the $p<0.1$ level). Grey indicates areas with no significant trends. The onset of significant and sustained warming on a 10- and 50-year timescale is printed on each plot.

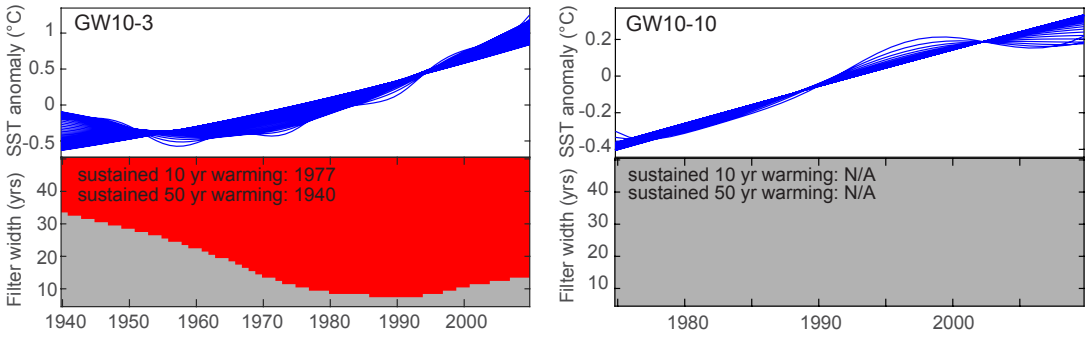

Figure S6. SiZer plots for the individual coral cores that contributed to the Wolf composite, GW10-3 and GW10-10. See Fig. S5 for an explanation of plot features.

Table S1. Details of individual Wolf Island cores and composite record.

Table S1
Summary of Wolf Island coral cores

	GW10-3	GW10-10	GW composite
Collection depth (m)	10	12	---
Core sampling length (mm)	868	610	---
Mean annual extension rate (mm/yr)	12.4	20.3	---
Record length	2010-1987; 1983-1940	2010-1985; 1982-1975	2010-1985; 1983-1940
Mean Sr/Ca (mmol/mol)	9.287	9.196	9.2478
Sr/Ca standard deviation	0.095	0.105	0.0923
Minimum Sr/Ca	8.944	8.866	8.9238
Maximum Sr/Ca	9.552	9.470	9.5196
Calibration parameters			
Sr/Ca-SST slope (standard error)	-0.058 (0.001)	-0.061 (0.001)	-0.057 (0.001)
Y-intercept (standard error)	10.732 (0.025)	10.728 (0.026)	10.658 (0.025)
r^2	0.57	0.50	0.64

Notes:
-Both Wolf Island cores have a death horizon representing a 2-3 year hiatus in growth following the 1982-83 El Niño
-Sr/Ca and SST statistics are calculated over the entire length of each core/composite; conversion from Sr/Ca to SST used the calibration equation derived for the composite (Sr/Ca=10.658-0.057*SST).
-Calibration parameters were derived by weighted least squares regression of Sr/Ca (mmol/mol) to OISST over the interval from May 1987-March 2010; compare to equations from Gagan et al. (2012), 11.278 - 0.084*SST, and Corrège (2006), 10.553 - 0.0607*SST.

References

Corrège, T. (2006), Sea surface temperature and salinity reconstruction from coral geochemical tracers, *Palaeogeography, Palaeoclimatology, Palaeoecology*, *232*(2-4), 408–428, doi:10.1016/j.palaeo.2005.10.014.

DeLong, K. L., T. M. Quinn, and F. W. Taylor (2007), Reconstructing twentieth-century sea surface temperature variability in the southwest Pacific: A replication study using multiple coral Sr/Ca records from New Caledonia, *Paleoceanography*, *22*(4), n/a–n/a, doi:10.1029/2007PA001444.

DeLong, K. L., T. M. Quinn, F. W. Taylor, C.-C. Shen, and K. Lin (2012), Improving coral-base paleoclimate reconstructions by replicating 350years of coral Sr/Ca variations, *Palaeogeography, Palaeoclimatology, Palaeoecology*, 1–19, doi:10.1016/j.palaeo.2012.08.019.

Fiedler, P. C., and L. D. Talley (2006), Hydrography of the eastern tropical Pacific: A review, *Progress in Oceanography*, *69*(2-4), 143–180, doi:10.1016/j.pocean.2006.03.008.

Gagan, M. K., G. B. Dunbar, and A. Suzuki (2012), The effect of skeletal mass accumulation in Porites on coral Sr/Ca and δ18O paleothermometry, *Paleoceanography*, *27*(1), 1–16, doi:10.1029/2011PA002215.

Howell, P., N. Pisias, J. Ballance, J. Baughman, and L. Ochs (2006), ARAND Time-Series Analysis Software, Available from: http://www.cricyt.edu.ar/paleo/softlib/arand/arand.html (Accessed 19 October 2015)

Johnson, G. C., B. M. Sloyan, W. S. Kessler, and K. E. McTaggart (2002), Direct measurements of upper ocean currents and water properties across the tropical Pacific during the 1990s, *Progress in Oceanography*, *52*(1), 31–61, doi:10.1016/S0079-6611(02)00021-6.

Julian, P. R., and R. M. Chervin (1978), A study of the Southern Oscillation and Walker Circulation phenomenon, *Mon. Wea. Rev.*, *106*, 1433–1451, doi:10.1175/1520-0493(1978)106<1433:ASOTSO>2.0.CO;2.

Kessler, W. S. (2006), The circulation of the eastern tropical Pacific: A review, *Progress in Oceanography*, *69*(2-4), 181–217, doi:10.1016/j.pocean.2006.03.009.

Linsley, B. K., P. Zhang, A. Kaplan, S. S. Howe, and G. M. Wellington (2008), Interdecadal-decadal climate variability from multicoral oxygen isotope records in the South Pacific Convergence Zone region since 1650 A.D, *Paleoceanography*, *23*(2), 1–16, doi:10.1029/2007PA001539.

Lukas, R. (1986), The termination of the equatorial undercurrent in the eastern Pacific, *Progress in Oceanography*, doi:10.1016/0079-6611(86)90007-8.

Mann, M. E., and P. D. Jones (2003), Global surface temperatures over the past two millennia, *Geophys. Res. Lett.*, *30*(15), 1–4, doi:10.1029/2003GL017814.

National Geophysical Data Center (2006), 2-minute Gridded Global Relief Data (ETOPO2) v2,,

doi:10.7289/V5J1012Q.

Nurhati, I. S., K. M. Cobb, and E. Di Lorenzo (2011), Decadal-Scale SST and Salinity Variations in the Central Tropical Pacific: Signatures of Natural and Anthropogenic Climate Change, *J. Climate*, *24*(13), 3294–3308, doi:10.1175/2011JCLI3852.1.

Reynolds, R. W., T. M. Smith, C. Liu, D. B. Chelton, K. S. Casey, and M. G. Schlax (2007), Daily High-Resolution-Blended Analyses for Sea Surface Temperature, *J. Climate*, *20*(22), 5473–5496, doi:10.1175/2007JCLI1824.1.

Sayani, H. R., K. M. Cobb, A. L. Cohen, W. C. Elliott, I. S. Nurhati, R. B. Dunbar, K. A. Rose, and L. K. Zaunbrecher (2011), Effects of diagenesis on paleoclimate reconstructions from modern and young fossil corals, *Geochimica et Cosmochimica Acta*, *75*(21), 6361–6373, doi:10.1016/j.gca.2011.08.026.

Schrag, D. P. (1999), Rapid analysis of high-precision Sr/Ca ratios in corals and other marine carbonates, *Paleoceanography*, *14*(2), 97–102, doi:10.1029/1998PA900025.

Strub, P. T., J. M. Mesias, V. Montecino, J. Rutillant, and S. Salinas (1998), Coastal ocean circulation off western South America, in *The Sea*, vol. 11, edited by A. R. Robinson and K. H. Brink, pp. 273–314, New York.

Thirumalai, K., A. Singh, and R. Ramesh (2011), A MATLAB™ code to perform weighted linear regression with (correlated or uncorrelated) errors in bivariate data, *J. Geol. Soc. India*, *77*(4), 377–380, doi:10.1007/s12594-011-0044-1.

Toggweiler, J. R., and K. Dixon (1991), The Peru Upwelling and the Ventilation of the South Pacific Thermocline, *J. Geophys. Res.*, *96*, 20,467–20,497.

Wallace, J. M., T. P. Mitchell, and C. Deser (1989), The Influence of Sea-Surface Temperature on Surface Wind in the Eastern Equatorial Pacific - Seasonal and Interannual Variability, *J. Climate*, *2*(12), 1492–1499, doi:10.1175/1520-0442(1989)002<1492:TIOSST>2.0.CO;2.

Wu, H. C., M. Moreau, B. K. Linsley, D. P. Schrag, and T. Corrège (2014), Investigation of sea surface temperature changes from replicated coral Sr/Ca variations in the eastern equatorial Pacific (Clipperton Atoll) since 1874, *Palaeogeography, Palaeoclimatology, Palaeoecology*, *412*(C), 208–222, doi:10.1016/j.palaeo.2014.07.039.

Zhang, G. J., and M. J. McPhaden (1995), The relationship between sea surface temperature and latent heat flux in the equatorial Pacific, *J. Climate*, *8*(3), 589–605, doi:10.1175/1520-0442(1995)008<0589:TRBSST>2.0.CO;2.